143
5-14-81
JWA

(2)

LR. 2644

RH324

ornl

ORNL/TM-7783

OAK
RIDGE
NATIONAL
LABORATORY

UNION
CARBIDE

MASTER

Iso-Response Contours in the ETF Neutral-Beam Injectors

J. M. Barnes
R. T. Santoro
R. A. Lillie
R. G. Alsmiller, Jr.

OPERATED BY
UNION CARBIDE CORPORATION
FOR THE UNITED STATES
DEPARTMENT OF ENERGY

Table of Contents

ABSTRACT

Iso-response contours in the Engineering Test Facility (ETF) neutral beam injector have been calculated for the neutron flux, nuclear heating in SS-316 and G10 insulation, biological dose rate, and the $^{58}Ni(n,p)^{58}Co$ and $^{59}Co(n,\gamma)^{60}Co$ reactions. The spatial dependence of these responses in the injector, in the shielding that surrounds it, and in the injection duct is presented.

I. INTRODUCTION

In a previous paper (Ref. 1), the results of two-dimensional radiation transport calculations to estimate the effects of neutron and gamma-ray streaming on the performance of the Engineering Test Facility (ETF) neutral beam injectors were reported. The nuclear heating rate in the cryopumping panels, the dose rate to the ion gun insulators, and the biological dose rate as a function of injector duct shielding were presented.

In this paper, iso-response contours as a function of spatial location in the ETF neutral beam injector-injection duct assembly are presented for a few selected nuclear responses. Data of this type are useful to design engineers for estimating the spatial dependences of the radiation throughout the system and for determining the optimum location and dimensions of shielding.

The details of the calculational model and the procedures used to generate the iso-response contours are given in Section II and the results are presented and discussed in Section III.

II. DETAILS OF THE CALCULATION

The two-dimensional model of the ETF, neutral beam injector assembly, and the shielding used in this study are shown in Fig. 1. The components are modeled in r-z geometry with cylindrical symmetry about the axis of neutral beam injection. The ETF plasma region and the neutral beam injection duct are each surrounded by a 120-cm-thick shield comprised of 65 v/o stainless steel type 316 and 35 v/o water with 6 w/o natural boron added. The sides and rear of the neutral beam injector are covered with 120 cm of concrete shielding. The components inside of the injector (bending magnet, cryopanels, calorimeter, baffles, etc.) and the procedures

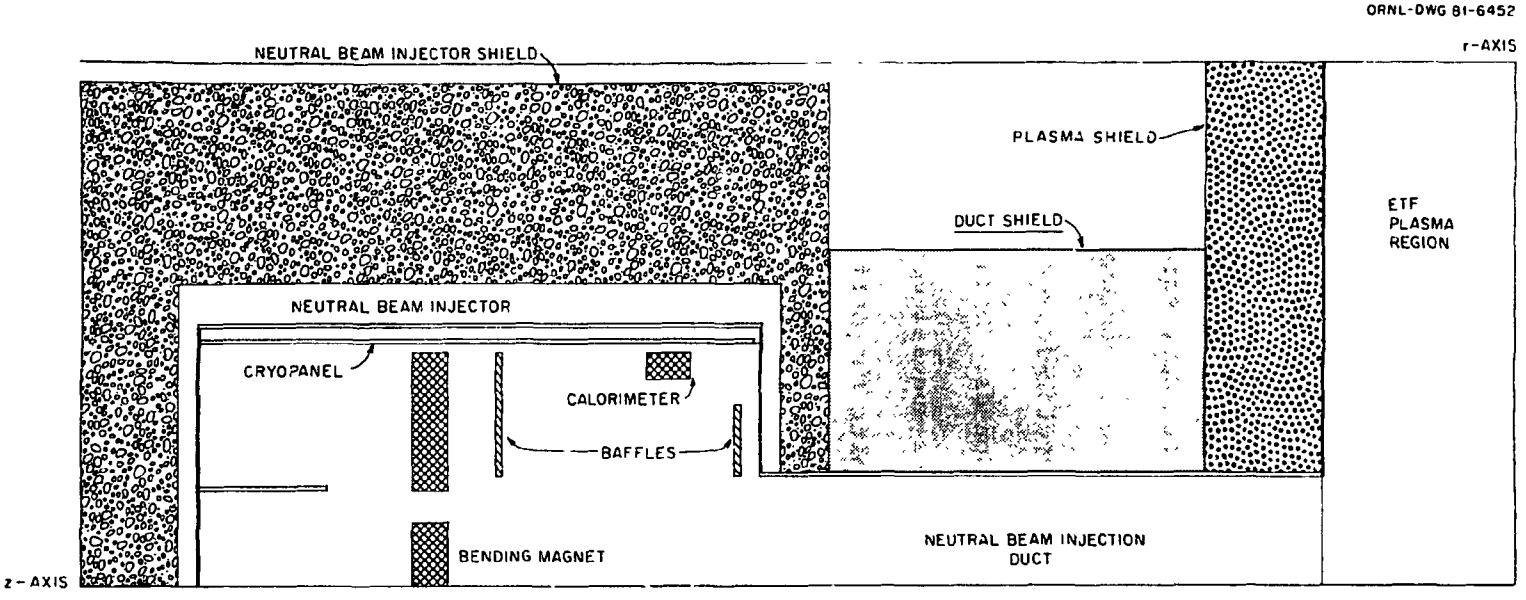

Fig. 1. Two-Dimensional Model of the ETF and Neutral Beam Injector Assembly.

used to incorporate these into the two-dimensional model are discussed in Ref. 2.

Several things must be noted in the model shown in Fig. 1. The scales used to represent the components in the radial and axial directions are not the same, so the components appear to be truncated along the z-axis. Also, the origin of the coordinate system is at the right in this figure, as well as in the contour plots presented in Section III. Neutral particle flow is left-to-right and radiation streaming from the plasma is right-to-left. The computer code used to generate the contours of constant response is constrained to function with the geometry represented in this manner.

The iso-response data were obtained by convoluting the energy and spatial distributions of the neutron and gamma ray flux distributions calculated in Ref. 1 with the appropriate response functions. The energy and spatial distributions of the radiation were obtained using the two-dimensional discrete ordinates code DOT IV.[3] Separate calculations were performed to treat the radiation from two sources: that which streams directly from the plasma into the injector and that which undergoes collisions in the reactor and duct shielding before entering the injector. The first region was taken to be the volume of the plasma which is viewed from a point on the duct centerline at the injector entrance. The radiation originating in this volume was taken to be a point source at the intersection of the plasm and the injector duct centerline. The second source region is the remaining plasma volume which was approximated using a ring source located at a radial distance of 103 cm from the intersection of the plasma and duct centerlines. The calculational procedure and

methods to obtain the particle distribution in these two sources is described in detail in Ref. 1. Both source terms include 14 MeV neutrons from the DT reactions in the plasma along with low-energy neutrons and secondary gamma rays that are present in the plasma volume as the result of 14-MeV neutron collisions and reactions in the materials surrounding the plasma.

For the ETF operating at 1140 MW, the total number of particles from the point source is 1.64×10^{19} particles/second and 1.27×10^{20} particles/second from the ring source. The neutron and gamma ray flux distributions in the mesh were obtained for 35 neutron energy groups and 21 gamma ray energy groups. For the purpose of this analysis, the spatial and energy-dependent fluxes for particles of type i obtained for the point (P) and ring (R) sources were combined to form a single distribution. That is

$$\phi_i(r,z,E) = \phi_i^P(r,z,E) + \phi_i^R(r,z,E) \qquad (1)$$

where i = neutrons or gamma rays. The spatial distribution of any nuclear response to neutrons or gamma rays is calculated from

$$R_i(r,z) = \int_E \phi_i(r,z,E) K_i(E) dE \qquad (2)$$

where $K_i(E)$ is the response function for particles of type i at energy E. These data serve as input to the code ISOPLT[4] which interpolates among the responses in space and magnitude to produce iso-contours throughout the geometric mesh used to describe the system.

III. DISCUSSION OF RESULTS

Contours of the instantaneous fast neutron flux (>13.5 MeV) and instantaneous total neutron flux in the ETF neutral beam injector assembly and shielding are plotted in Figs. 2 and 3, respectively. The fast neutron flux is attenuated by nearly seven orders of magnitude in the stainless steel type 316 plus borated water shielding that surrounds the plasma region and the injection duct. The total neutron flux is reduced by about six orders of magnitude in these shields. Except at the rear of the neutral beam injector, the flux values just outside of the shielding are $\sim 10^8 n/cm^2/s$ for all neutrons. The radiation streaming directly into the injector from the point source representation of radiation emitted from the viewed volume passes through the hole in the magnet and leads to a hot spot at the rear of the injector. The fast and total neutron fluxes outside of the shielding behind the injector are two orders of magnitude greater than that leaking through the shielding along the side of the injector.

The instantaneous total nuclear heating rate (due to neutrons and gamma rays) and the instantaneous heating rate due to gamma rays only are shown in Figs. 4 and 5. These data were obtained using the kerma factor for stainless steel type 316 as the response function in Eq. (2). The contours in both figures are very similar in both shape and magnitude. This similarity arises because the gamma heating dominates the nuclear heating. The instantaneous heating rate in the neutral beam injector cryopanel reported in Ref. 1 showed that the contribution to the heating rate from neutrons is only about 5% of the total heating rate. The profiles in Figs. 4 and 5 indicate that the instantaneous heating rate in the

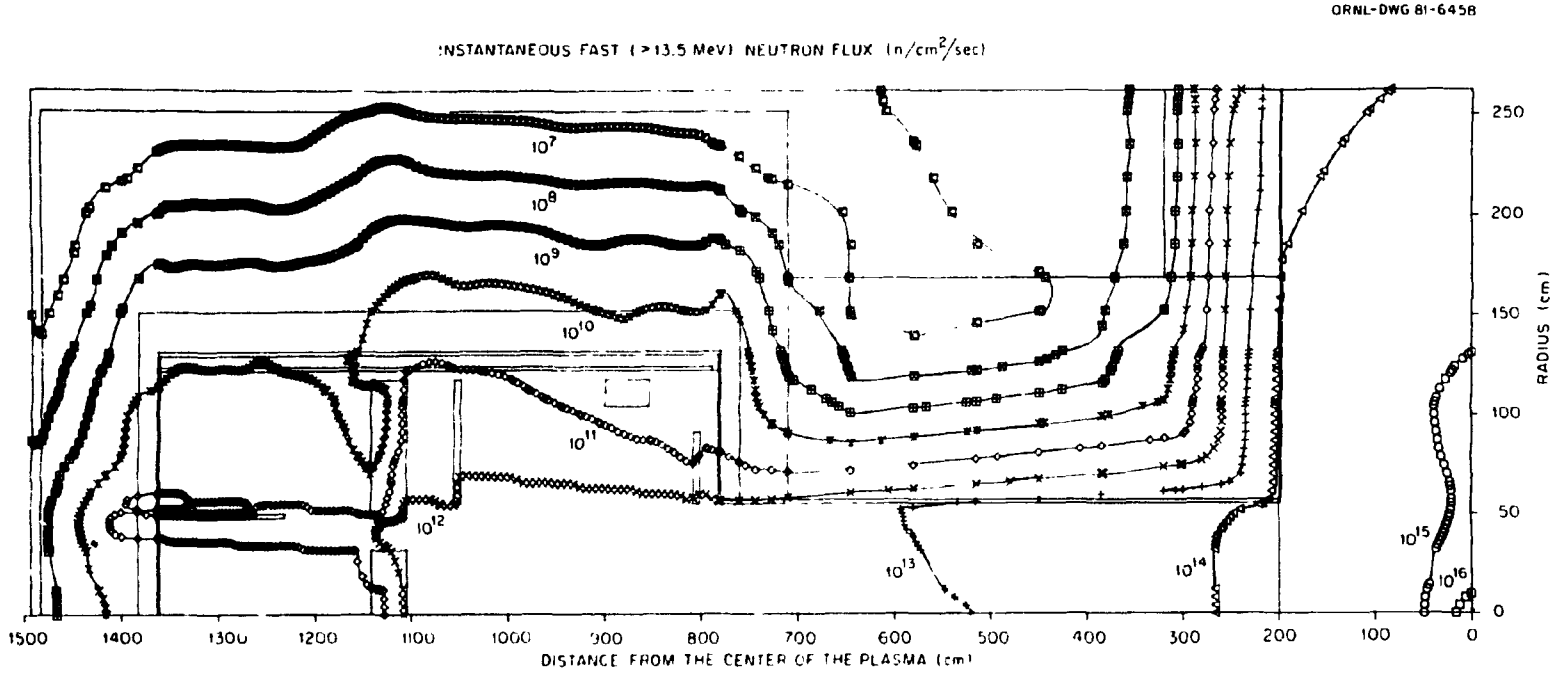

Fig. 2. Contours of Constant Neutron Flux for Neutrons Having Energies Above 13.5 MeV.

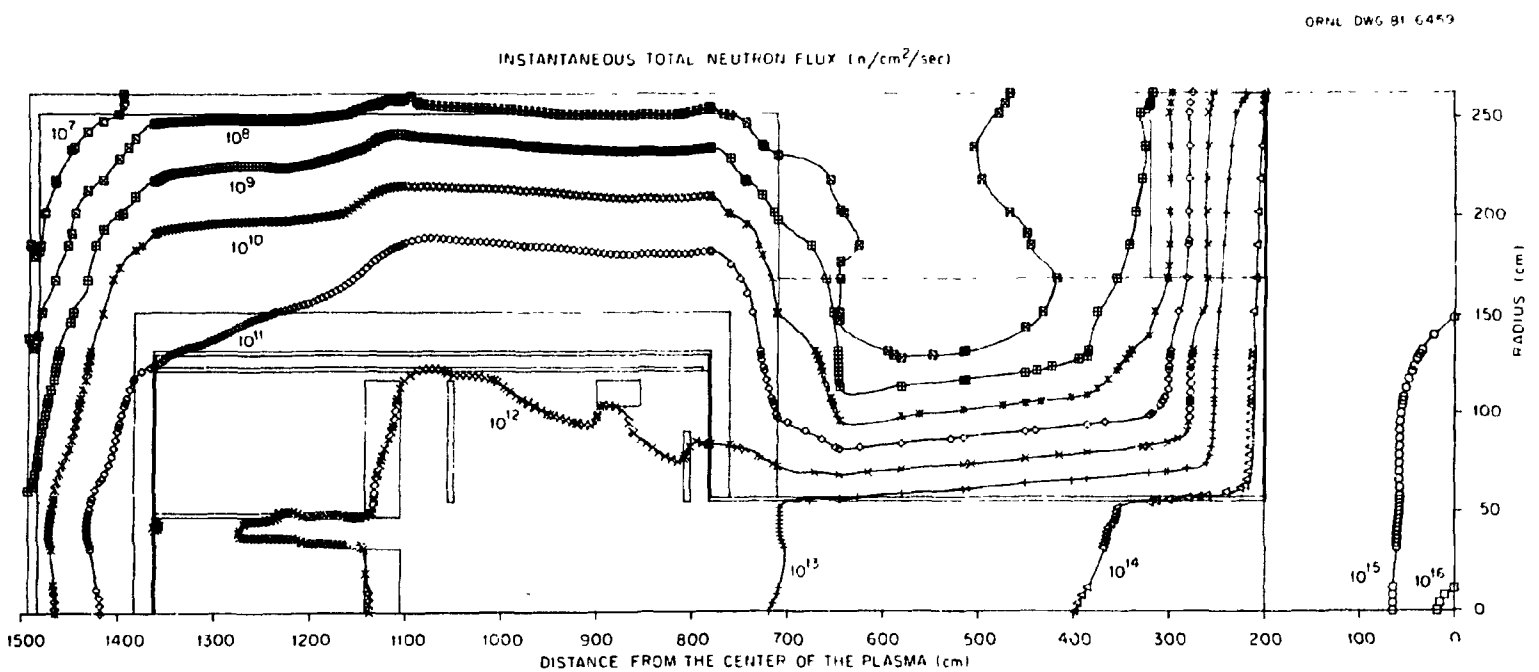

Fig. 3. Contours of Constant Total Neutron Flux.

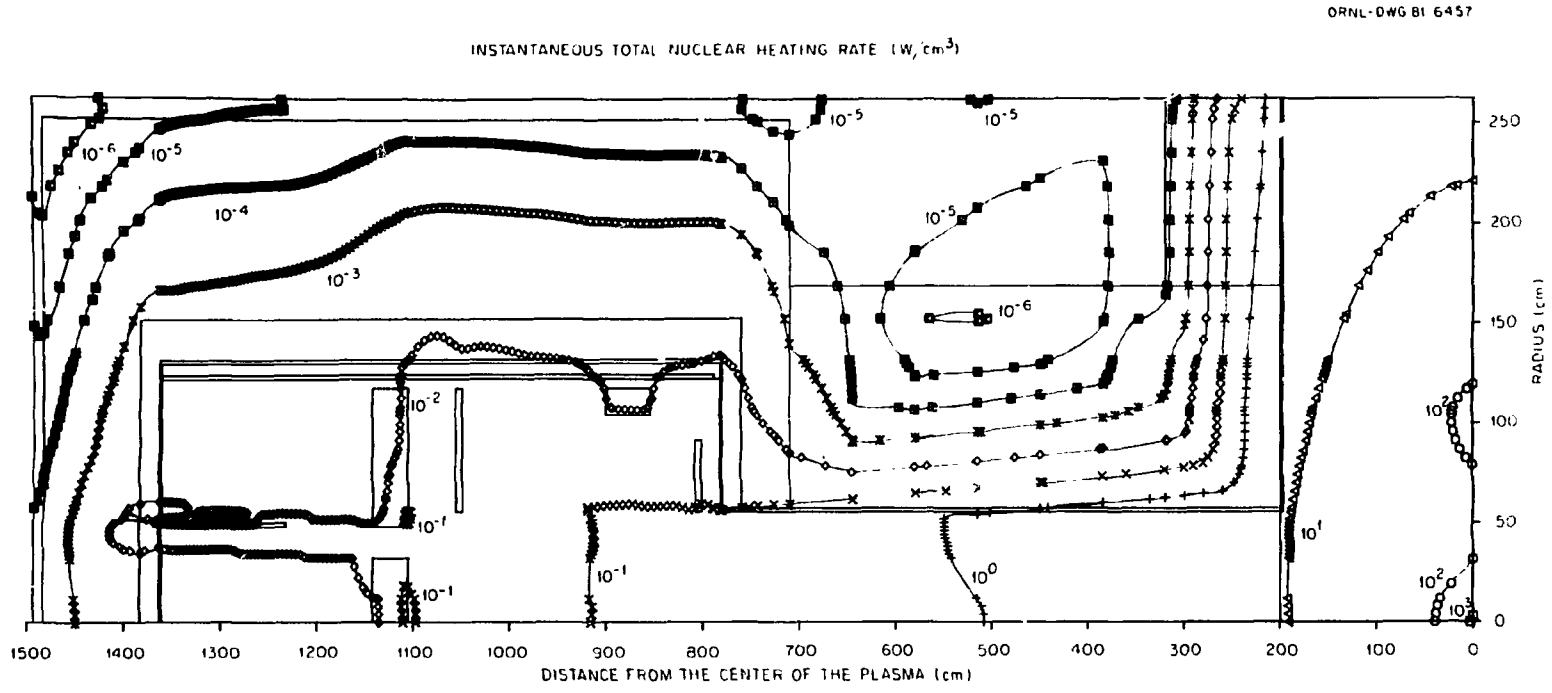

Fig. 4. Contours of Constant Total Nuclear Heating Rate in SS-316.

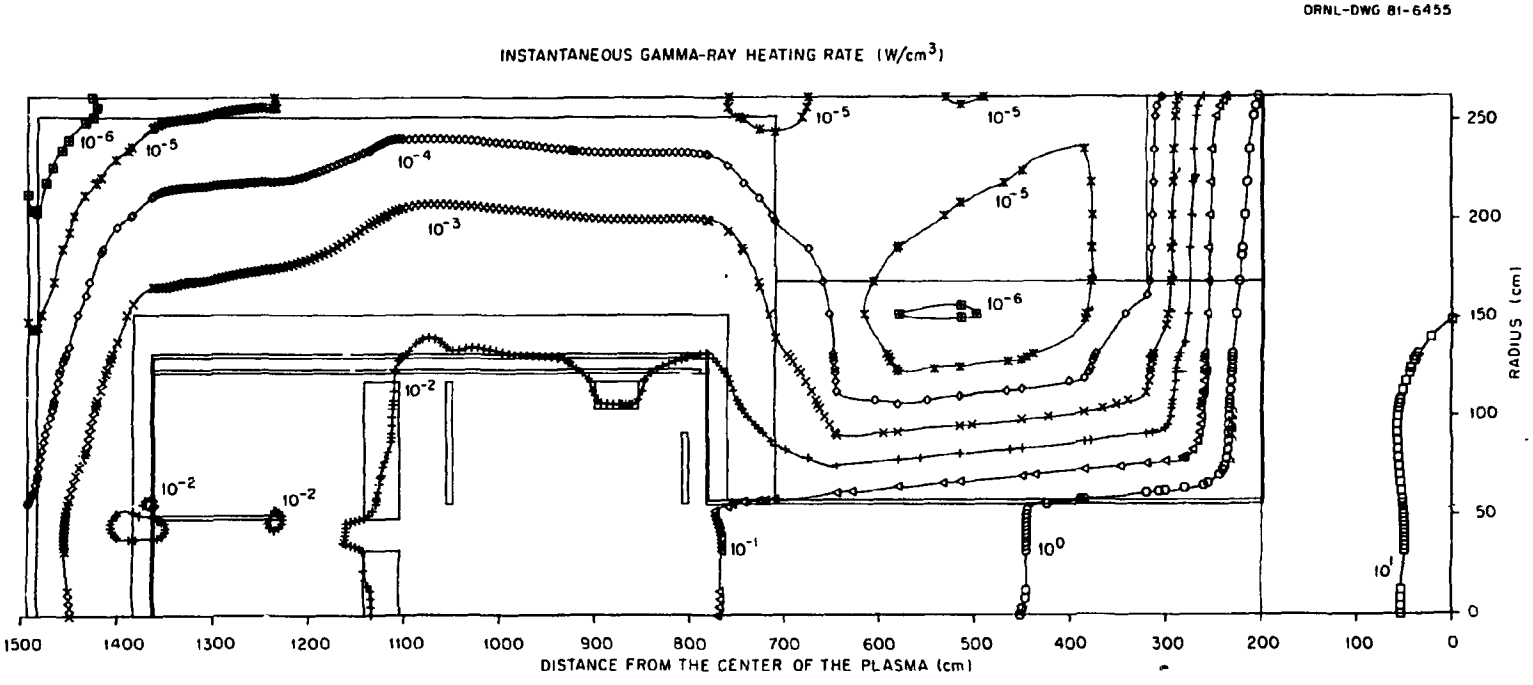

Fig. 5. Contours of Constant Gamma Ray Heating Rate in SS-316.

cryopanels is of the order of 10^{-2} w/cm^3. Some localized heating occurs in the bending magnet and along the neutralizer tube at the rear of the injector. There is also some localized heating in the vicinity of the ion guns at the rear of the injector.

The total nuclear heating rate contours in the neutral beam injector obtained when the kerma factor for the insulating material G10 is used as the response function in Eq. (2) are plotted in Fig. 6. These data were obtained assuming that G10 is present everywhere in the neutral beam injector and shielding. Since G10 is a likely candidate as the insulating material for use in the ion guns or other components requiring electrical insulation, these data are useful in estimating the lifetime of the insulation since the material dose rate can be inferred from the heating rate data.

The instantaneous total biological dose rate in the system is shown in Fig. 7. The dose rate outside of the shielding is $\sim 10^6$ mrem/h except at the rear of the injector where the radiation streaming from the plasma causes the dose equivalent rate to be higher by two orders of magnitude.

Figures 8 and 9 show the contours of constant reaction rate for the ^{58}Ni(n,p), ^{58}Co and ^{58}Co(n,γ) ^{60}Co transmutation reactions. The data were obtained by using the microscopic cross sections for the reactions as the response function in Eq. (2). The atomic densities for ^{58}Ni and ^{59}Co have not been included in the calculation of these responses, so the actual volumetric reaction rate may be obtained by multiplying the reaction rate in the figure by the number density of the target nuclei in the material of interest.

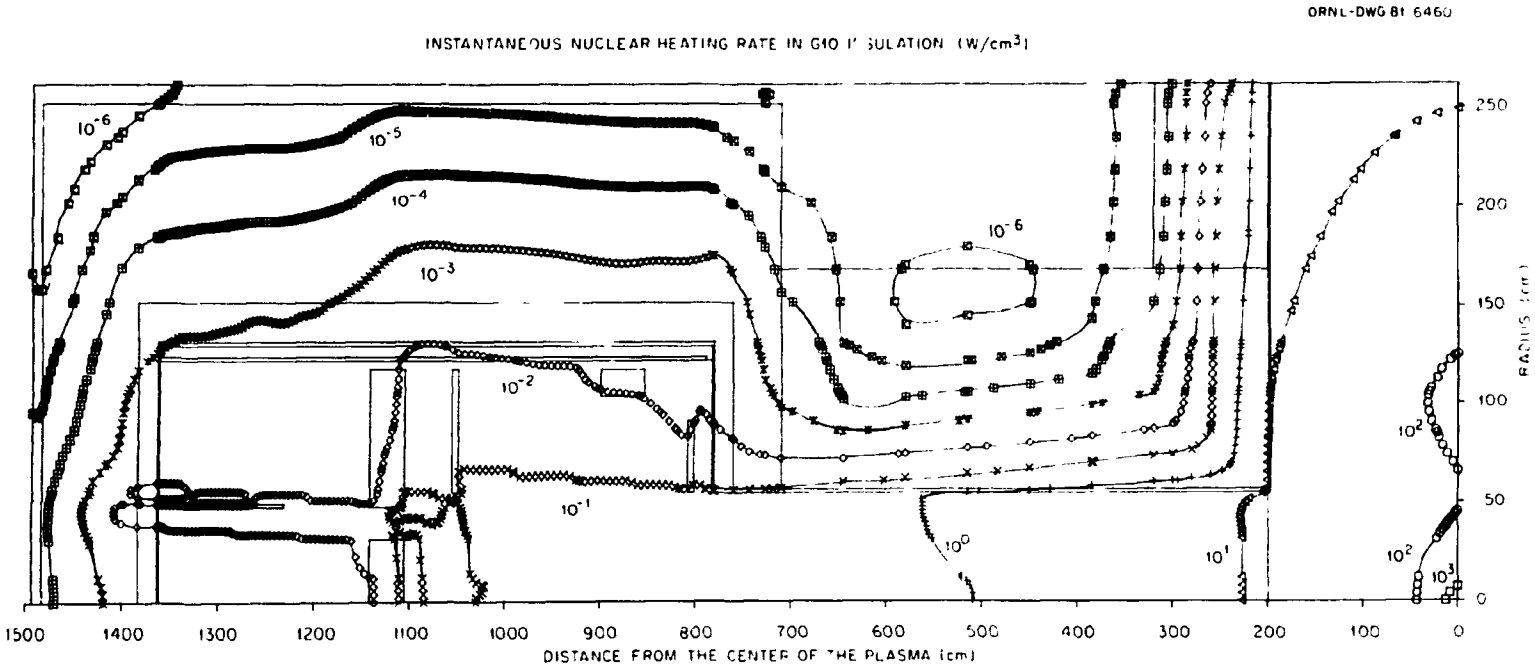

Fig. 6. Contours of Constant Heating Rate in G10 Insulation.

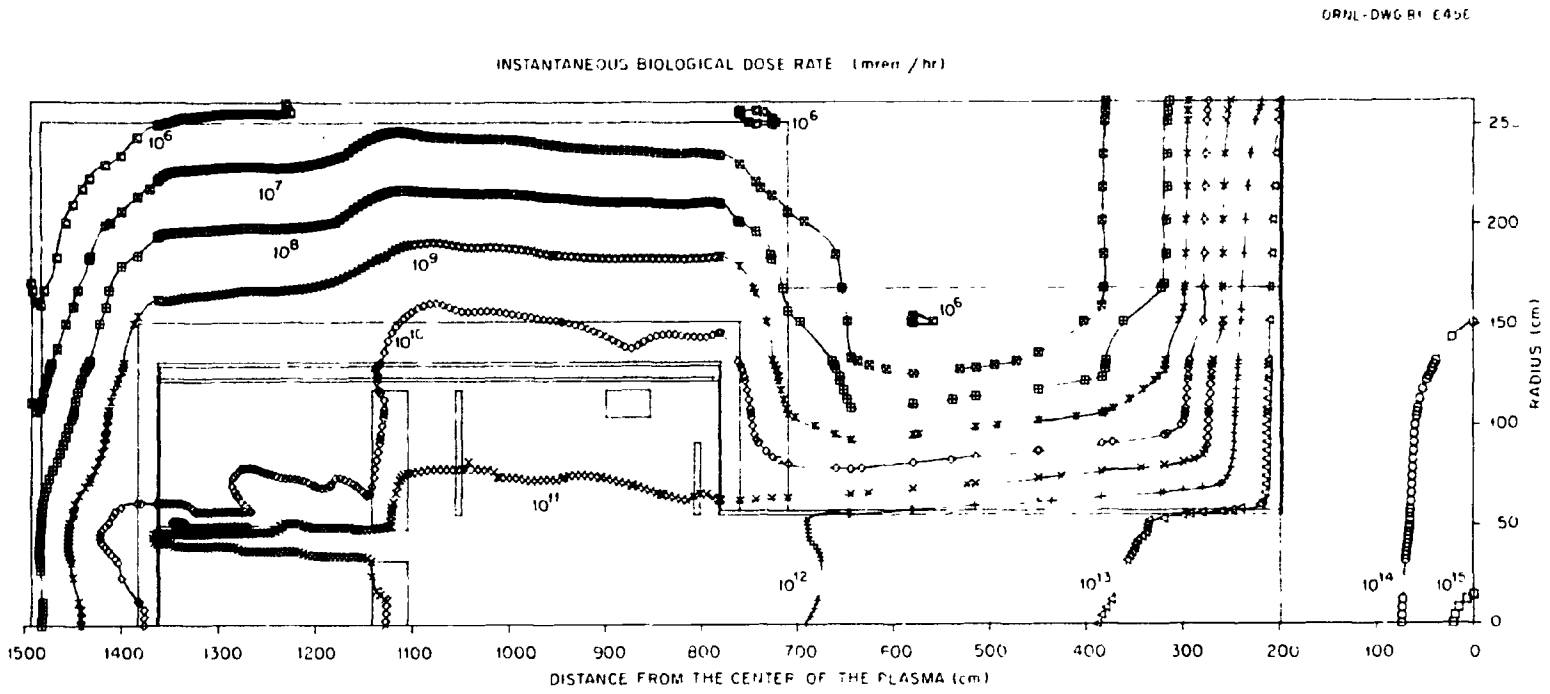

Fig. 7. Contours of Constant Instantaneous Total Biological Dose Rate.

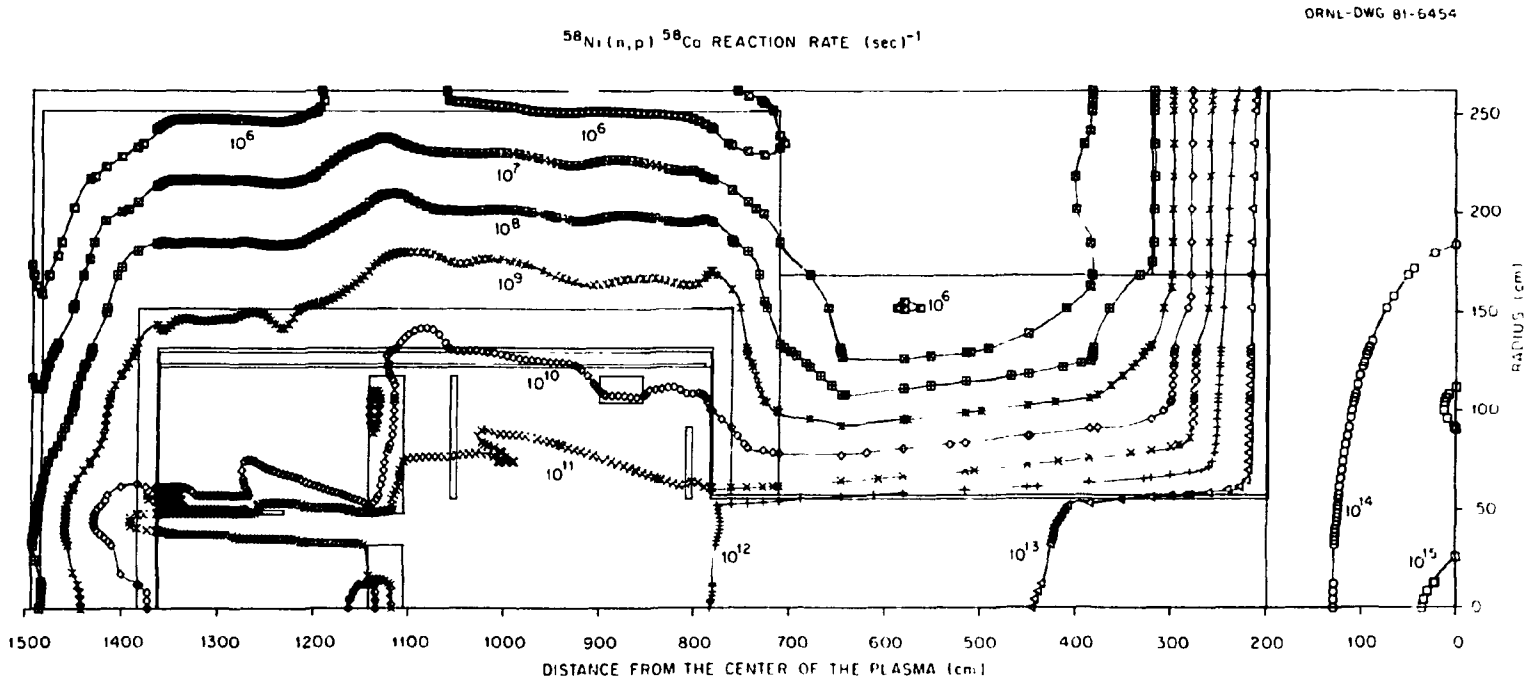

Fig. 8. Contours of Constant $^{58}Ni(n,p)^{58}Co$ Reactions.

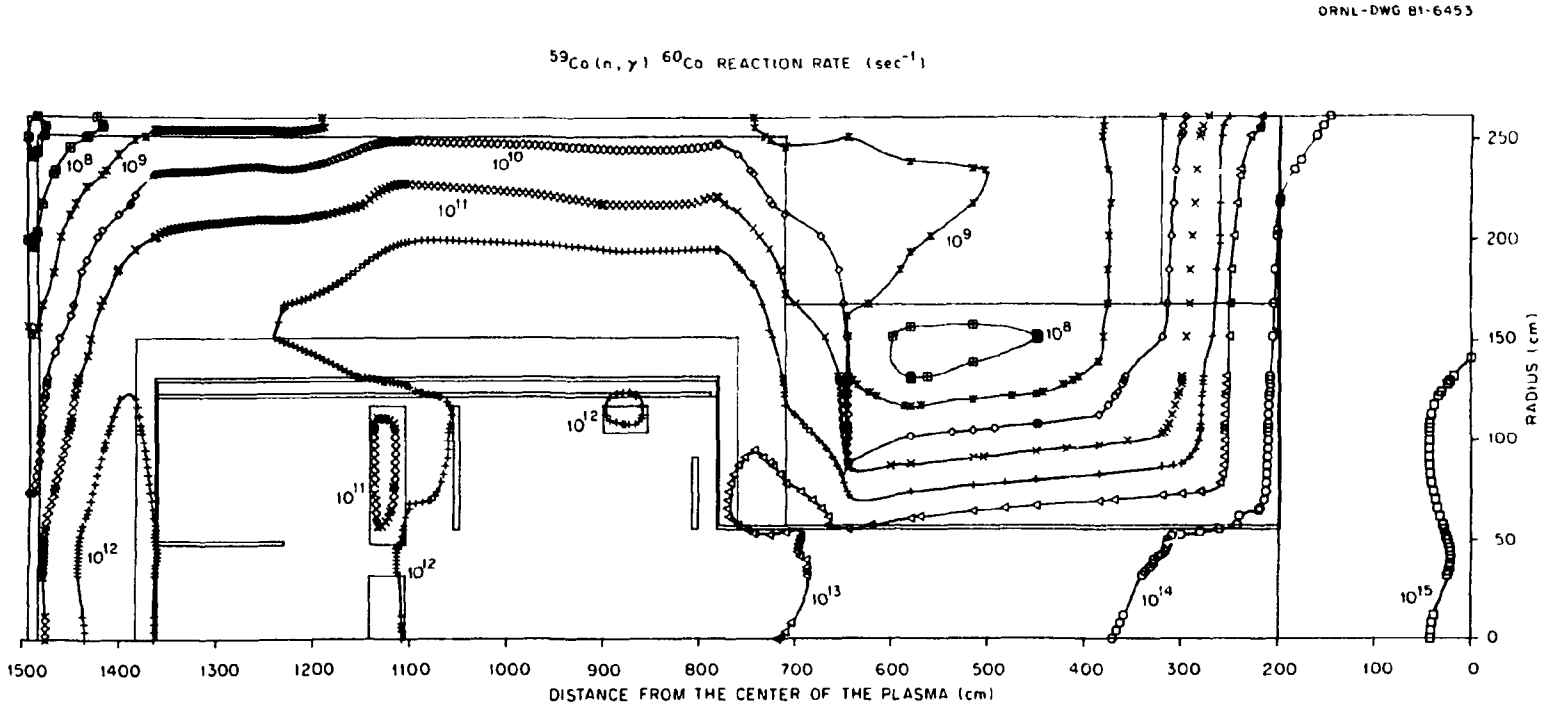

Fig. 9. Contours of Constant $^{59}Co(n,\gamma)^{60}Co$ Reactions.

REFERENCES

1. R. A. Lillie, R. T. Santoro, R. G. Alsmiller, Jr. and J. M. Barnes, "Neutron and Gamma-Ray Streaming Calculations for the ETF Neutral Beam Injectors," Oak Ridge National Laboratory Report, ORNL/TM-7705 (1981).

2. R. T. Santoro, R. A. Lillie, R. G. Alsmiller, Jr. and J. M. Barnes, Nucl. Sci. Eng. 60, 225 (1979).

3. W. A. Rhoades, D. B. Simpson, R. L. Childs and W. W. Engle, Jr., "The DOT-IV Two-Dimensional Discrete Ordinates Transport Code with Space Dependent Mesh and Quadratures," Oak Ridge National Laboratory Report, CRNL/TM-6529 (1979).

4. D. T. Ingersoll and C. O. Slater, "DOGS - A Collection of Graphics for Support of Discrete Ordinates Codes," Oak Ridge National Laboratory Report, ORNL/TM-7188 (1980).